Published in Surface Science 384, issues 1-3, 36-45, 1997
which should be used for any reference to this work

Real space mapping of the surface atomic environment via low energy scattering spectroscopy

R.G. Agostino *, P. Aebi, J. Osterwalder [1], J. Hayoz, L. Schlapbach

Institut de Physique, Université de Fribourg, Pérolles, CH-1700 Fribourg, Switzerland

Abstract

Low-energy ion scattering spectroscopy is used to obtain real space surface imaging of the atomic surroundings of different fcc metal surfaces. Scattered He^+ ions were mapped over a large solid angle sector. By using an universal shadow cone expression, it is possible to invert the angular maps into two-dimensional real space maps. The inversion procedure is tested on Pt(111), Cu(001) and Al(111) surfaces getting nearest neighbour atoms up to a distance of 4 Å. Furthermore, for known surfaces the maps also allow to extract information on the scattering mechanism itself.

Keywords: Aluminium; Copper; Ion scattering spectroscopy; Ion–solid interaction; Platinum; Surface structure

1. Introduction

Low-energy ion scattering spectroscopy (LE-ISS) is a well-known technique for surface analysis. Bombarding a surface with noble gas ions of some hundred of eV and measuring the energy and angular distributions of the recoiled ions, the elemental composition and structure can be determined.

The technique is based on the fact that the elastic scattering of the incoming ions is the prevalent mechanism for their change in energy and momentum. At energies from 100 to 10 keV the classical theory of ISS considers the ion–surface scattering as a sequence of elastic two-body collision events. In this model, each ion reflected by the surface experiences an energy loss as a consequence of elastic scattering while the influence of the surrounding atoms is neglected. Hence, for a given scattering angle, its final energy is directly related to the mass of the target atom. By acquiring energy spectra of the reflected ions an elemental analysis of the surface can be carried out [1–3].

On the other hand, the noble gas ions which penetrate the surface or suffer multiple collisions are readily neutralised owing to their high electron affinity ($E_{1s}(\mathrm{He}) = 24.6\,\mathrm{eV}$) compared to the work function of the sampled materials. Consequently, they are not detected by the electrostatic energy analysers typically used in ISS. This effect together with the large cross section for elastic scattering, makes ion scattering spectroscopy sensitive to the topmost atomic layer [1–3].

Angle resolved ISS is widely used to determine nuclear positions in real space. Examples are the measurement of adatom positions relative to the

* Corresponding author. Fax: +41 26 300.97.47; e-mail: raffaele.agostino@unifr.ch

[1] Permanent address: Physik-Institut, Universität Zürich-Irchel, CH-8057 Zürich, Switzerland.

surface [4], the determination of nearest neighbour distances and the evaluation of the surface order [5]. These methods offer great flexibility due to the broad range of useful energies and incoming ion masses [2].

In the literature we find only few studies where the surface order is determined by a complete angular mapping of the scattered ions and/or neutrals [6]. A well established method for the inversion of such complete angular maps into real space atom coordinates is not yet available. For the interpretation of the azimuthal and polar scans, several methods use trajectory calculations with different interaction potentials between incoming ions and surface atoms [1]. These molecular dynamics methods lead to the direct interpretation of the intensity features along high symmetry directions. Additional fine structure showing up in complete angular maps of scattered ions, however, are not considered because of the great amount of computing time necessary [1].

In the present work we demonstrate how new insight can be obtained applying a new data representation in terms of real space coordinates. The method is based on the binary collision approximation using the Molière potential [7] for the ion–atom interactions. In particular, we show the following:

(1) Taking advantage of the continuous polar and azimuthal angle-scanning of the ion beam incidence-angle we are able to give a real-space map of ordered surfaces.

(2) The interpretation of various fine structure features is much easier and direct when complete (θ_{in}, ϕ_{in}) angle maps are available.

(3) For known surface structures, we can get information on the surface scattering mechanism.

Furthermore, the mapping procedure is tested for different target atom masses, different low index surfaces and different incidence ion beam kinetic energies.

2. Experimental method

The analysis system is based on a modified Vacuum Generator ESCALAB Mk II spectrometer [8] with a base pressure of 2×10^{-11} mbar, equipped with a three channeltron hemispherical electrostatic energy analyser, a Mg Kα and Si Kα twin anode X-ray source, a quadrupole mass spectrometer and a low-energy electron diffraction (LEED) system. The ion beam was produced by a VG AG 60-185 Ion Gun with a nominal angular spread of 0.2°. In the present experiment the feed gas for the ion gun is He (99.997% pureness). During operation, a liquid nitrogen trap is activated on the He line in order to purge the He gas from residual impurities. With the ion beam on, the partial pressure in the analysis system is 2×10^{-8} mbar. The relative angle between the fixed ion gun and analyser is 90° giving a scattering angle of $\theta_{sc} = 90°$ (Fig. 1). X-ray photoelectron spectroscopy and LEED are used to check the surface cleanliness and order, respectively.

The sample is mounted on a *xyz* manipulator with 2 rotational axes. Rotations are motorised and computer controlled such that the incidence polar angle θ_{in} (with respect to the surface) and azimuthal angle ϕ_{in} can be swept over the whole hemisphere above the sample (Fig. 1) and a series of energy spectra can be recorded automatically on a predetermined set of angles (θ_{in}, ϕ_{in}).

The nominal analyser energy resolution is 1% of its pass energy which can vary from 0.1 to 200 eV. We used the maximum pass energy because the present study was performed on clean surfaces where only one element is present on the surface and, consequently, only one peak is present in the

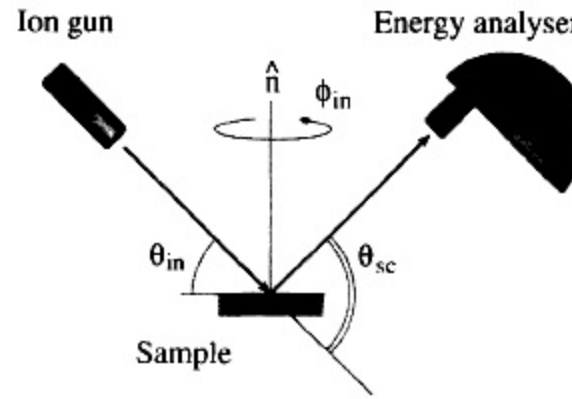

Fig. 1. Schematic representation of the experimental geometry. The scattering angle θ_{sc} is fixed to 90° while the incidence angles θ_{in} and ϕ_{in} can vary continuously by rotating the sample.

ISS energy spectra. The angular resolution is regulated by a system of slits inside the energy analyser and it is fixed in this experiment to 2°.

The experimental procedure consists in the acquisition of the intensity of the ISS peak associated with a specific target atom for each (θ_{in}, ϕ_{in}) setting. Intensities are recorded for up to 4000 angular settings. The sample normal, the analyser direction and the incident beam direction are coplanar for all the angular settings. The geometrical arrangement is such that the surface normal points to the analyser entrance slits when the incident beam is parallel to the surface (Fig. 1). For the scattering angle $\theta_{sc}=90°$, the energy E_1 of the He^+ reflected ions is determined by $E_1=E_0\,(M-4)/(M+4)$ where M is the mass of the scatterer atom on the surface and E_0 the ion beam kinetic energy [1].

The acquisition of a complete angular map takes up to 90 min. In order to evaluate the surface damage caused by sputtering we monitored the LEED pattern. For all the studied surfaces, the diffraction spots are still sharp after the data acquisition even though a higher inelastic background intensity is visible. On the other hand, we scan the ion beam on a 0.5 cm^2 area and the typical sample current is below 10 nA. On this basis, we conclude that the surface damage is usually small although it could become a major problem for time consuming measurements.

3. Theoretical background

It is well known that the single binary collision approach is sufficient for the elemental analysis of surfaces [1–3]. On the other hand, we need to consider two events in order to understand the features of angle resolved measurements. The first one is a focusing event in which the weakly deflected ion trajectories become more dense on a cone around a first target atom (Fig. 2a). As a consequence, the incoming ion flux is zero behind the atom and at the maximum on the wall of the so-called shadow cone. The second event is the large-angle scattering of the incoming ions into the analyser. When rotating the sample, each time a neighbour atom passes through the shadow cone

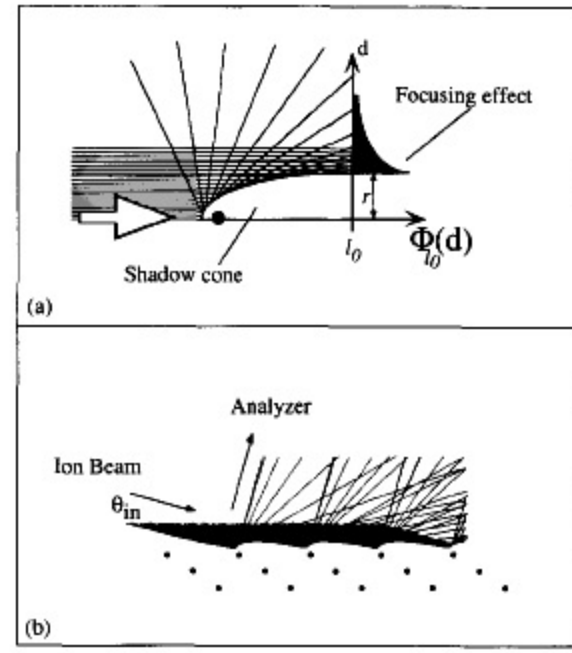

Fig. 2. (a) The ion scattering mechanism is producing an "ion-free" shadow cone beyond the target atom. Small angle scattering events lead to a focusing of the incoming trajectories on a shadow cone wall: the ion flux Φ vs distance d from the shadow cone centre $\Phi(d)$ is peaked in correspondence with the cone radius r. (b) Large angle scattering events are enhanced when the nearest neighbour atom is placed on the shadow cone of the target atom. The effect is amplified for close packed rows.

wall produced by the first scatterer (Fig. 2b), the probability of large angle scattering events increases giving rise to a maximum in the intensity of reflected ions. The whole process is still labelled "single" or "quasisingle scattering" because the first event changes only slightly the energy and the momentum of the incoming ion. For a fixed scattering geometry, the scattered ion energy is mainly determined by the mass of the second scatterer.

In angle-resolved ISS, at very grazing incidence ($\theta_{in}\approx 0$) each surface atom lies in the shadow cone of its neighbour and the large angle scattering intensity is practically negligible. At a critical angle θ_c a drastic increase of the scattering intensity due to quasisingle scattering events involving surface atoms takes place (Fig. 3a). The critical polar angle θ_c is strictly related to the scattering geometry involving atoms in a chain, corresponding to the situation where the second scatterers pass through

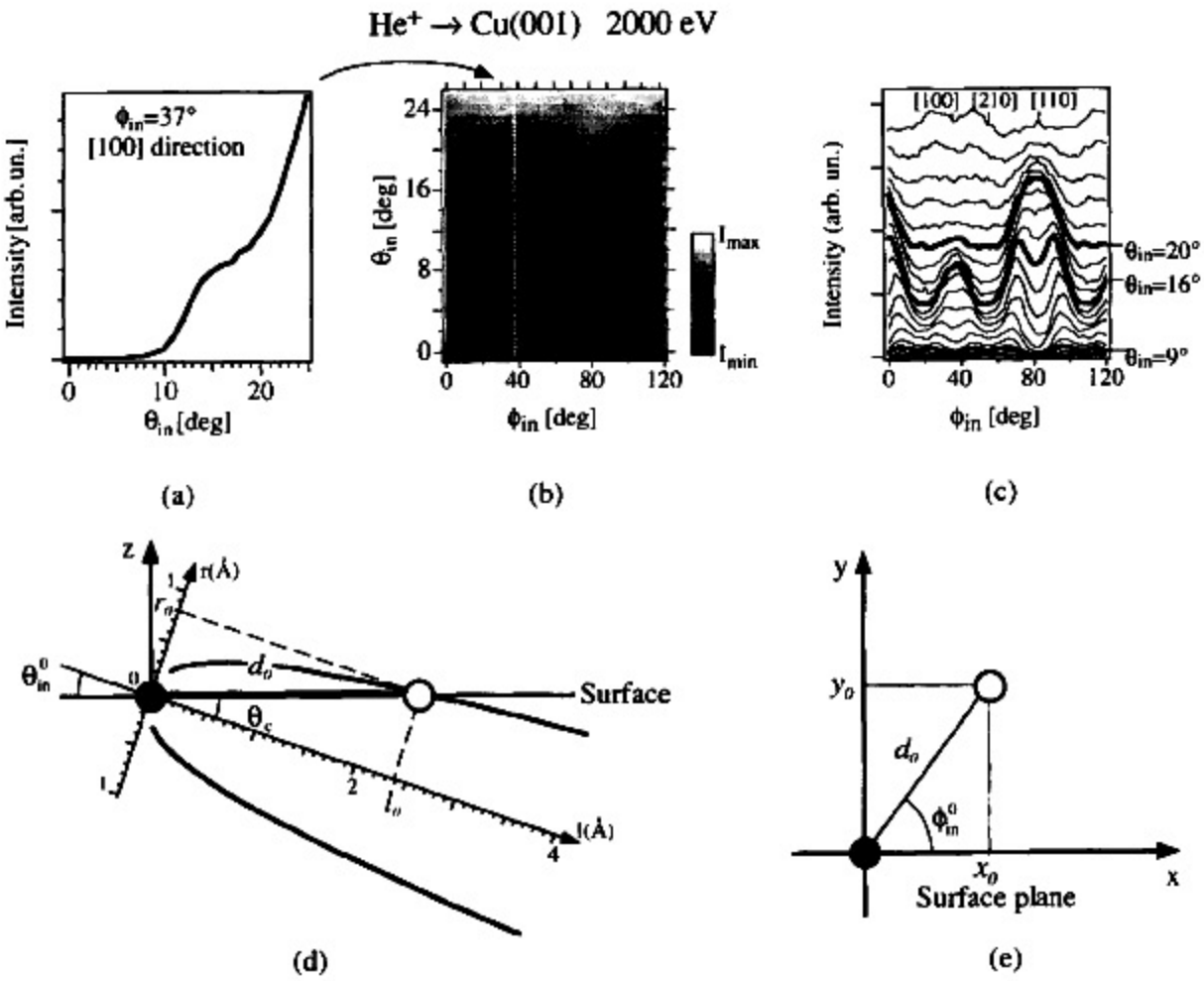

Fig. 3. (a) An example of polar scan $I\phi_{in}(\theta_{in})$ for the Cu peak intensity for the 2000 eV $He^+ \rightarrow Cu(001)$ system. The azimuth is fixed along the [100] surface direction. (b) Greyscale representation of the angular map $I(\theta_{in}, \phi_{in})$ for the 2000 eV $He^+ \rightarrow Cu(001)$ system. The vertical dotted line indicates the polar scan shown in (a). (c) Azimuthal scans collected on a 120°-azimuthal sector above a Cu(001) sample in a waterfall representation. The He^+ ion energy is 2000 eV. The incidence polar angle step is 1° while the azimuthal angle step is 2°. The curves obtained at 9°, 16° and 20° are shown with a thicker line (see text). (d) The shadow cone radius r vs the distance l beyond the surface target atom (filled circle) after the Oen formulas for He^+ ions impinging with a kinetic energy of 2000 eV on a Cu atom. The incidence polar angle θ^0_{in} is chosen to correspond to the critical angle θ_c for an atom (empty circle) at the distance d_0 located at (l_0, r_0) on the shadow cone $r(l)$. (e) Knowing the shadow cone form and the impact polar angle θ_c it is possible to determine the distance between the first (small-angle) scatterer and a second (large-angle) scatterer. The azimuthal angle ϕ^0_{in} defines the x_0 and y_0 coordinates of the second scatterer within the surface plane.

the cone walls. When the incidence polar angle θ_{in} is greater than the critical angle θ_c for nearest neighbour atoms, the large angle scattering events involve exclusively the atomic layers below the first one.

In a series of polar scans we can identify the critical angle for every azimuthal direction. In fact, in the series of polar scans as displayed in a grey-scale representation in Fig. 3b, a distinct intensity enhancement occurs between 15° and 19° depending on the azimuth. For comparison, the series of azimuthal scans equivalent to Fig. 3b are plotted in Fig. 3c using the traditional representation of angle-resolved ISS.

Knowing the form of the shadow cone radius $r(l)$ (Fig. 3d), with l the distance beyond the first scatterer, the critical angle can be determined as $\theta_c = \arctan(r_0/l_0)$ with an associated distance $d_0 = \sqrt{r_0^2 + l_0^2}$. In general, we can pass from the relation $r(l)$ for the shadow cone to the function $d(\theta_{in})$ for the surface atoms. Having the distance between a pair of surface atoms and its azimuthal direction ϕ_{in} we are able to locate the second scatterer in the x–y real-space plane, i.e. we find its relative coordinates $x_0 = d_0 \cos(\phi_{in})$, $y_0 = d_0 \sin(\phi_{in})$ where ϕ_{in} is the azimuthal angle with respect to a fixed surface direction (Fig. 3e).

Once an $I(\theta_{in}, \phi_{in})$ map of the scattering intensity (Fig. 3b) is obtained over a large solid angle and the form of the shadow cone (Fig. 3d) is known we can perform a mapping into the x–y real-space plane. Starting from a (x, y) mesh (Fig. 3e) of surface coordinates we calculate the corresponding d_0 and ϕ_{in}^0 for each couple (x_0, y_0). Finally, we invert $d(\theta_{in})$ in order to find θ_{in}^0. With θ_{in}^0 and ϕ_{in}^0, the intensity to be plotted at (x_0, y_0) is found by interpolating the experimental $I(\theta_{in}, \phi_{in})$ (Fig. 3b).

It is clear that the important factor for the mapping procedure is the knowledge of the shadow cone shape. In the first approximation, $r(l)$ is calculated using the Coulomb interaction between the Z_1 electrons of the ion and the Z_2 electrons of the target atom. In this case the shadow cone form is a simple parabola $(r(l) = 2\sqrt{bl}$ with $b = (Z_1 Z_2 e^2)/(E_0))$ and the function $d(\theta_{in})$ is $d(\theta_{in}) = (4b)/(\tan^2\theta_{in})\sqrt{1 + \tan^2\theta_{in}}$. In the last decades several models have taken corrections to the Coulomb potential into account [2]. In 1983, Oen calculated a universal expression for the classical shadow cone formed behind an atom [7]. He used the Molière screened potential with a screening length a, given by the Lindhard formula $a = 0.4685(Z_1^{2/3} + Z_2^{2/3})^{-1/2}$ [9]. It is then possible to determine the shadow cone radius r as a function of the distance l behind the target atom. The formulas are given below and referred to as the Oen formulas

$$(r)/(2\sqrt{bl}) = 1 - 0.12\alpha + 0.01\alpha^2 \qquad (1)$$

where $0 \leq \alpha \leq 4.5$,

$$(r)/(2\sqrt{bl}) = 0.924 - 0.182\ln(\alpha) + 0.0008\alpha \qquad (2)$$

where $4.5 \leq \alpha \leq 100$, with $\alpha = 2\sqrt{bl}/a$ and E_0 the incoming ion energy. The inversion of these formulas is no more possible to find out analytically the dependence of θ_{in} from d and a numerical approach is used in the inversion procedure. Notice that the formulas do not contain adjustable parameters.

The shadow cone radius varies over a broad range. It becomes large when the projectile and target atom masses are high or the incoming ion kinetic energy is low. Using He^+ ions as projectiles we have, for example, large radii for scattering from a Pt surface or using small kinetic energies.

In the complete (θ, ϕ) maps features of enhanced intensity can be observed over a wide range of angles in the complete (θ, ϕ) maps. However, high intensity cannot always be interpreted as positions of atoms in real-space as described before, because of the finite dimension of the shadow cone wall. Such effects, appearing away from the high symmetry directions, will be discussed below.

4. Results and discussion

In Fig. 3c azimuthal scans are plotted for a set of polar angles on a 120°-azimuthal sector. He^+ ions of 2000 eV are used on Cu(001). In the angle-resolved curves we can recognise the usual features of an ISS experiment: the azimuthal scan at $\theta_{in} = 9°$ shows minima along the [100] and [110] directions for $\phi_{in} = 36°$ and $\phi_{in} = 81°$, respectively. A shallow minimum is located at 54° pointing along the [210] direction. Notice, however, that along [110] an intensity maximum is reached around $\theta_{in} = 20°$ and in the [100] direction this happens around $\theta_{in} = 16°$. Qualitatively this is in accord with the expected higher incidence angle for intensity enhancement along the closer packed rows.

In order to corroborate the inversion procedure described in the preceding section we will examine in the following several systems, varying the target atom mass, the ion kinetic energy and the surface geometry. $I(\theta_{in}, \phi_{in})$ maps such as those of Fig. 3b are acquired on Pt(111) for He^+ ion energy at 1000 and 2000 eV and on Al(111) at 500 eV.

4.1. Cu(001)

Fig. 4a reports the ISS real-space mapping of the Cu(001) surface acquired using He^+ ions with a kinetic energy of 2000 eV. The $I(x, y)$ values are obtained as described in Section 3. A 10 Å-square area is mapped around the first scatterer, i.e. the shadow cone "producer". A distance range from 1.65 to 5.0 Å corresponds to a variation of the incidence polar angle θ_{in} from 25° to 12°. The range below 1.65 Å (or above 25° incidence angle) was not mapped in order to avoid second layer contributions. For each θ_{in} the complete azimuthal range is measured with an azimuthal step of 1°. On the top-right part of the image, circles are placed at the ideal atom position around the central scatterer.

Analysing the picture we can fix our attention on the feature labelled A. Performing a radial cut (Fig. 4b) from the central scatterer, i.e. the shadow cone producer, along the [110] direction we have an intensity enhancement which reaches its maximum at a projected distance d equal to 2.49 Å. This is repeated for all symmetry related ⟨110⟩ directions. We assign the feature A to the ion scattering enhancement due to the transit of the nearest neighbour through the shadow cone of the central scatterer. In other words A is the image of the nearest neighbour whose ideal position is at 2.56 Å, i.e. 0.07 Å away from the position revealed by ISS mapping. Each pair of surface atoms aligned in this direction is contributing to the signal. Repeating the same procedure for the ⟨100⟩ directions (Fig. 4b) we find maxima of intensity such as B at 3.55 Å from the centre. This corresponds to the second nearest neighbour (the ideal distance is 3.61 Å). We emphasise that the positions are determined using only the Oen formulas without any further data treatment. The width along the radial directions of the features A and

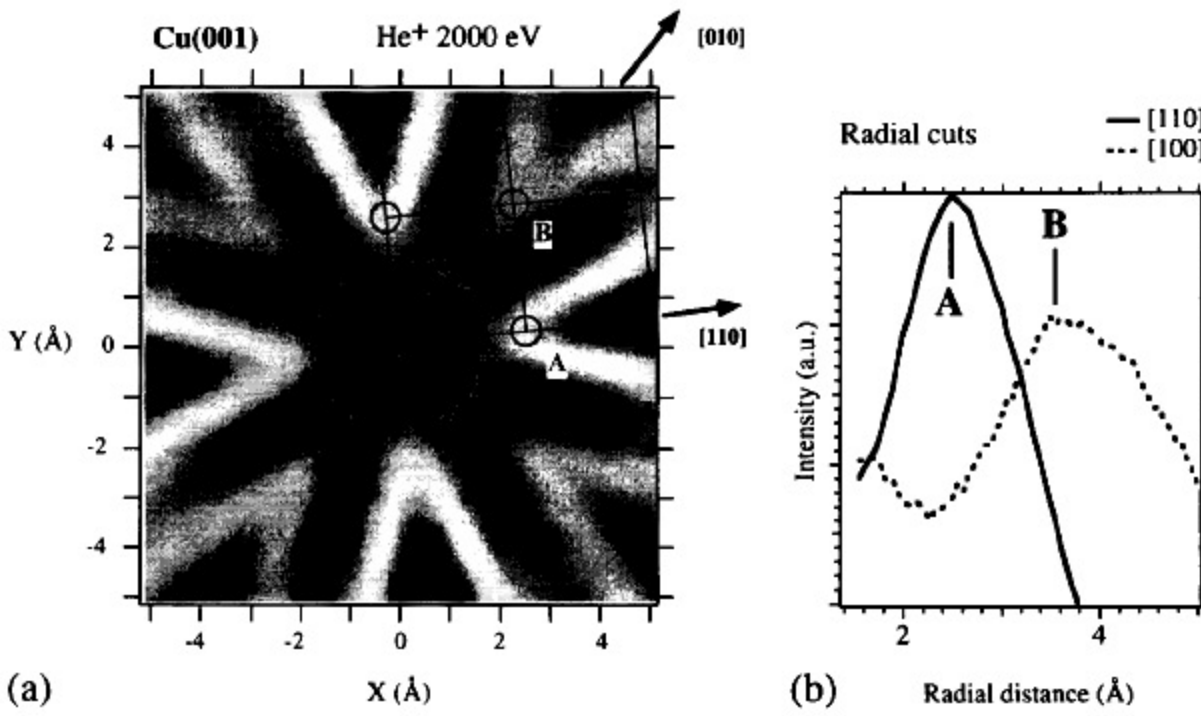

Fig. 4. (a) ISS map of the Cu(001) surface obtained by inverting the $I(\theta_{in}, \phi_{in})$ map acquired using 2000 eV He^+ ions. Intensity is given in greyscale where black (white) corresponds to intensity minimum (maximum). On the right side of the map, solid line circles are placed around the true surface atom positions and the [110] and [100] directions are indicated by arrows. The map is obtained following the procedure described in the text. The raw data are averaged exploiting the 4-fold symmetry and a smooth background is removed. Only the region for $d > 1.65$ Å is reported. (b) Radial cuts along the [110] and [100] direction indicated in (a).

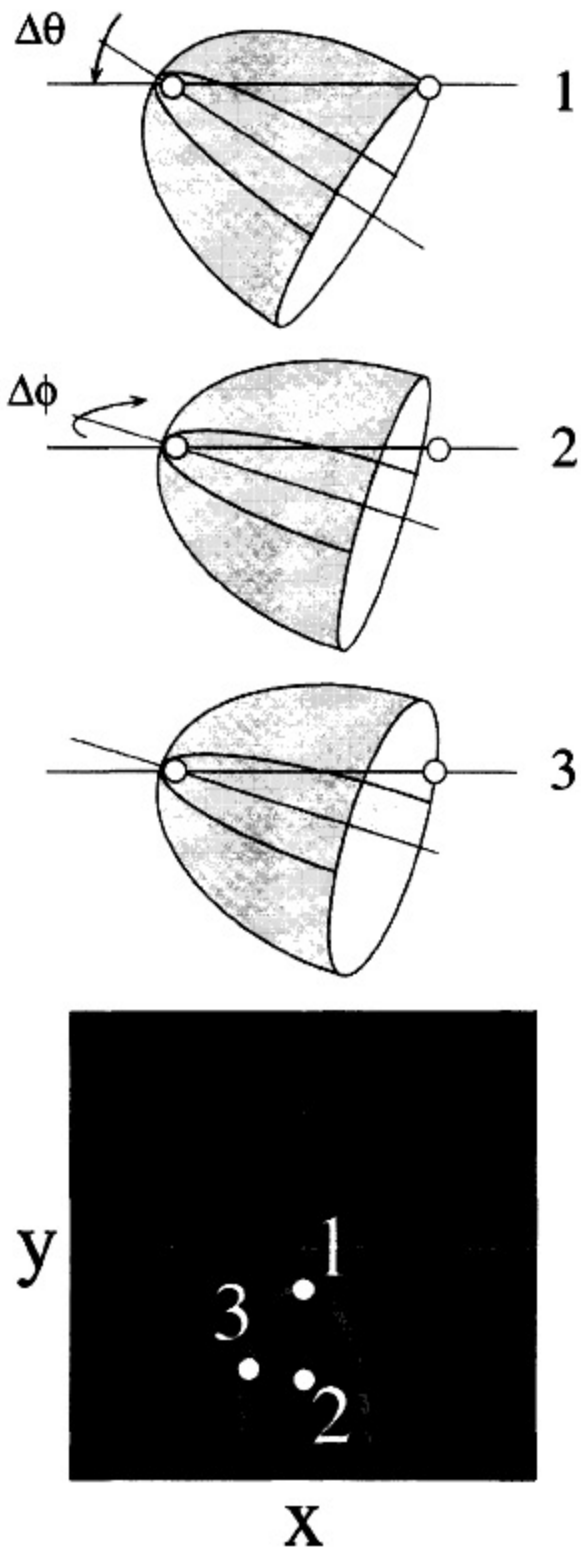

B results from the intrinsic width of the trajectory focusing region around the shadow cone convoluted with the effects of atomic vibrations [1] and the finite angular resolution of the analyser. A quantitative evaluation of the relative importance of these effects is beyond the aim of this work.

The map shows the presence of high intensity features with a parabolic form. The apices of the parabola are placed on the features labelled A, B and equivalent points. The scattering events generating these structures are closely related to those we associate to the features A and B. Fig. 5 helps to understand the origin of these structures. We start from the geometry in which the beam lies in the plane containing the normal and the [110] direction of the surface. Performing a polar scan we have the maximum associated with the nearest neighbours at the critical incidence polar angle θ_c (Fig. 5, step 1). From this position we can decrease θ_{in} by $\Delta\theta$. Doing this we put the nearest neighbour inside the shadow cone (Fig. 5, step 2). Consequently, the signal intensity falls towards zero. It is sufficient to increase (or decrease) the incidence azimuthal angle by $\Delta\phi$ fixing the incidence polar angle, to move the shadow cone again on top of the nearest neighbour (Fig. 5, step 3). An angle variation by $\Delta\theta$ and $\Delta\phi$ corresponds to an increase of the radial distance (1→2) and a subsequent tangential movement at a fixed radial distance (2→3). By varying ($\Delta\theta$, $\Delta\phi$) continuously, keeping the neighbouring atoms on the shadow cone, we obtain the parabolic curve starting from the features A or B in Fig. 4. The existence of these parabolic curves is another argument for the assignment of features A and B to the images of nearest neighbours.

From the shape of these parabolic curves we can obtain information on the scattering process

Fig. 5. Scheme depicting the mechanism at the origin of the parabolic structures in the ISS maps (see text). Upper panel: changes of the impact angles, $\Delta\theta$ (1→2) and $\Delta\phi$ (2→3), and the corresponding impact geometry changes are shown. In positions 1 and 3 the first atom focuses the incident ions on the second one (high scattering intensity) while in position 2 the second atom is hidden from the first (low scattering intensity). In the lower part of the panel the 1, 2 and 3 conditions are depicted in the projected surface map.

itself. In fact, the limiting value of $\Delta\phi$ for θ_{in} going to zero, i.e. d going to infinity, is the angular opening of the shadow cone at the nearest neighbour distance behind the first scatterer. From the azimuthal scans at very grazing incidence (Fig. 3b and c) we get the FWHM of the parabola apertures which result in $38\pm1°$ and $30\pm1°$ for the features A and B, respectively. Hence, we can deduce that for He^+ ions at 2000 eV the shadow cone radius at a distance of 2.56 Å from a Cu atom for He^+ ion at 2000 eV is 0.83 ± 0.05 Å and at 3.61 Å it is 0.93 ± 0.05 Å [10]. These values are very close to those predicted by the Oen formulas. These results are summarised in Table 1.

4.2. Pt(111)

In the second experiment (He^+ scattering on the Pt(111) surface) we studied the influence of the close-packing together with different scattering conditions. As a matter of fact, the heavier Pt atoms ($Z_{Cu}=29$, $Z_{Pt}=78$) produce wider shadow cones while the surface is closer packed than in the Cu(001) case.

The ISS maps of the Pt(111) surface obtained using He^+ ions with a kinetic energy of 1000 and 2000 eV are presented in Fig. 6a and b, respectively. The radial distance ranges from 1.25 to 5 Å, corresponding to incidence polar angles ranging from 45° to 16° in the first case and from 37° to 13° in the second. Even though the scattering conditions are different from the previous situation, we obtain very similar features. In particular, the atomic position determined from the maxima along [110] directions is 2.76 Å at 1000 eV where as the ideal distance is 2.77 Å. From the parabolic intensity curves starting from the nearest neighbour images we find the shadow cone radius at 2.77 Å to be equal to 1.20 ± 0.05 Å. The ISS map of the same surface obtained at 2000 eV (Fig. 6b) gives nearest neighbour intensity maxima at 2.51 Å. The shadow cone radius at 2.77 Å is 1.01 ± 0.05 Å.

Comparing the maps obtained at the two energies we notice that at the higher energy the shadow cone parabola aperture behind the nearest neighbour is narrower leaving channels open for eventual next nearest neighbour scattering. In fact, we notice a wider high intensity region along the [$\underline{1}12$]-like directions in the 2000 eV map compared to the 1000 eV one. Cuts of the ISS map of Fig. 6b along the [$\underline{2}11$] and [$\underline{1}12$] directions are shown in Fig. 7. For distances from the centre larger than 3 Å there is an intensity increase which reaches its maximum at 4.47 and 4.68 Å, respectively. The next nearest neighbour (ideal distance 4.8 Å) images are then represented by these broad structures. The estimated nearest neighbours distance is systematically smaller in the real space maps. The reason for such an error comes from the fact that the model adopted in the present work is a binary collision model [2] in which the collision event is drastically simplified. All the possible inelastic effects, such as collective excitations in the solid induced by the incoming ions, are not considered. These effects are related to the interaction of the charge of the projectile with the electrons of the sample. They become important

Table 1

Surface	Experimental nn ISS max. position (Å)	Theoretical nn distance (Å)]	Experimental shadow cone radius (Å)	Theoretical shadow cone radius (Å)
Al(111) He^+ 500 eV	2.64	2.86	1.27 ± 0.05	1.12
Pt(111) He^+ 1000 eV	2.74	2.77	1.20 ± 0.05	1.20
Pt(111) He^+ 2000 eV	2.51	2.77	1.01 ± 0.05	1.00
Cu(001) He^+ 2000 eV	2.49	2.55	0.83 ± 0.05	0.83
Cu(001) He^+ 2000 eV	3.55	3.61	0.93 ± 0.05	0.93

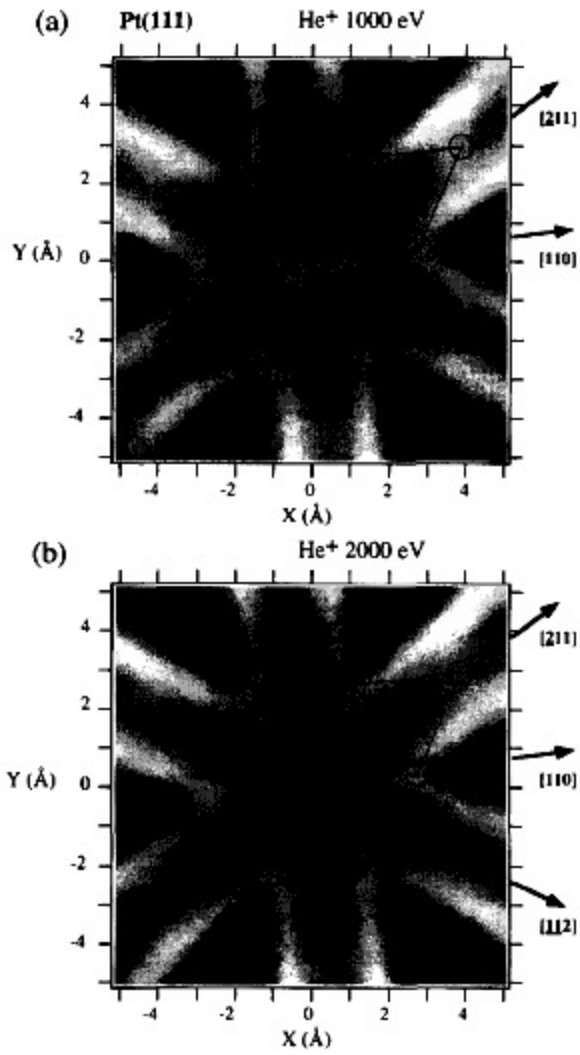

Fig. 6. Greyscale ISS maps of the Pt(111) surface obtained using He^+ ions at 1000 eV (a) and 2000 eV (b). The raw data are averaged exploiting the 3-fold symmetry and a smooth background is removed. Only the region for $d > 1.25$ Å for (a) and $d > 1.0$ Å for (b) is reported. Solid line circles are placed around the surface atom positions.

at higher projectile kinetic energies [2]. If we consider that the incoming ions lose part of their energy approaching to the sample surface, the actual shadow cone will be larger and the resulting nearest neighbour distance will be systematically under-estimated. Then, it is expected that the error increase with the kinetic energy of the ions and with the number of electrons of the target atoms.

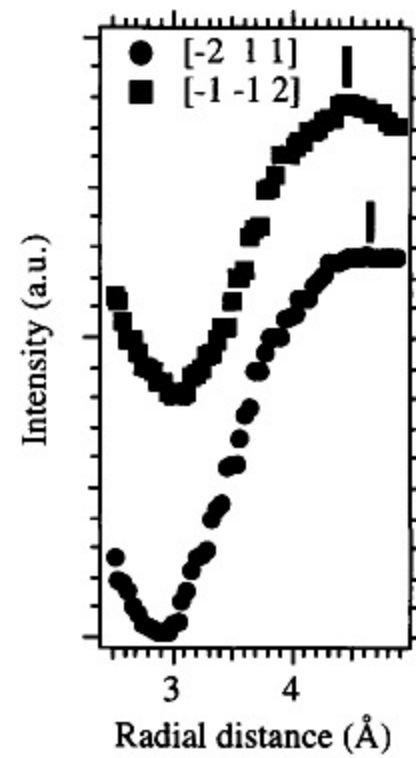

Fig. 7. Radial cuts of the Pt(111) map (He^+ 2000 eV) along the [2$\bar{1}$1] and [11$\bar{2}$] directions. The vertical ticks are placed in correspondence to the maxima.

Differences in the curves for distances lower than 3 Å are due to the second layer contributions which are appearing along the [2$\bar{1}$1] direction.

4.3. Al(111)

The Al(111) surface, finally, represents another limiting case because of the light atomic mass. We show in Fig. 8 the ISS mapping obtained using 500 eV He^+ ions. The map closely resembles those obtained for Pt(111) concerning symmetry and shape of the main features. The maximum of the ISS signal is located at 2.64 Å from the centre. The shadow cone radius at the nearest neighbour distance (2.86 Å) is 1.27 ± 0.05 Å.

5. Conclusions

A new method of mapping and analysing the angle-resolved ISS data is presented. We make use

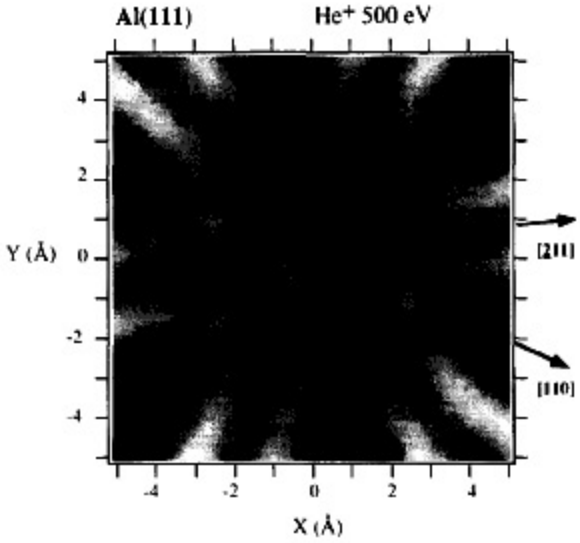

Fig. 8. Greyscale ISS map of the Al(111) surface obtained using He^+ ions at 500 eV. The raw data are averaged exploiting the 3-fold symmetry and a smooth background is removed. Only the region for $d > 1.0$ Å is reported. Solid line circles are placed around the surface atom positions.

of the universal shadow cone expression given by O.S. Oen to associate to each ion impact direction a (x, y) position on the surface map. The maps obtained for different fcc metal surfaces give quite precisely the neighbour atom positions up to 4 Å. Various fine features can be directly associated with the shape of the shadow cone. Studying these shadow cone images it is possible to extract information on the scattering process itself in terms of the shadow cone radius at known distances.

The accuracy of the described mapping method compares very well with the one of photoelectron holography and related methods developed in the past years [11–19]. In addition, ISS is a very surface sensitive spectroscopy. This makes our method very useful for studies concerning, e.g., the topmost layer reconstruction, surface alloying and thin film growth. Further improvements can be obtained by adapting existent ion-trajectory calculation codes in order to simulate the scattering patterns for complex surfaces where both, reconstruction and more than one chemical element is present.

Acknowledgements

The authors wish to thank R. Fasel for many stimulating discussions. Excellent technical support was provided by O. Raetzo, E. Mooser, F. Bourqui, C. Neururer and H. Tschopp. The present work is partially supported by the Fonds National Suisse pour la Recherche Scientifique.

References

[1] M. Aono, Nucl. Instr. and Meth. in Phys. Res. B 2 (1984) 374.
[2] P.G. Bertrand, J.W. Rabalais, in: J.W. Rabalais (Ed.), Low Energy Ion–Surface Interactions, J. Wiley and Sons, Chichester, England, 1994, ch. 2, pp. 55-116.
[3] H. Niehus, W. Heiland, E. Taglauer, Surf. Sci. Rep. 17 (1993) 213 and references therein.
[4] R.H. Bergmans, A.L.G.P. Brands, A.W. Denier Van der Gon, W.C.A.N. Ceelen, H.H. Brongerma, P. Bielen, C. Creemers, Surf. Sci. 350 (1996) 1.
[5] M.M. Sung, J.W. Rabalais, Surf. Sci. 342 (1995) L1137.
[6] H. Niehus, K. Mann, B.N. Eldridge, M.L. Yu, J. Vac. Technol. A 6 (1988) 625.
[7] O.S. Oen, Surf. Sci. 131 (1983) L407.
[8] D. Naumović, A. Stuck, T. Greber, J. Osterwalder, L. Schlapbach, Phys. Rev. B 47 (1993) 7462.
[9] J. Lindhard, Kgl. Danske Videnskab. Selskab Mat. Fys. Medd. 14 (1965) 34.
[10] The radius r is found according to $r = a_0 \sin(\alpha/2)$ where a_0 is the atom–atom distance and α is the measured FWHM of the parabola opening angle.
[11] J.J. Barton, Phys. Rev. Lett. 67 (1991) 3106.
[12] S.Y. Tong, H. Li, H. Huang, Phys. Rev. Lett. 67 (1991) 3102.
[13] V. Fritzsche, D.P. Woodruff, Phys. Rev. B 46 (1992) 16128.
[14] D.K. Saldin, X. Chen, N.C. Kothari, M.H. Patel, Phys. Rev. Lett. 70 (1993) 1112.
[15] J. Osterwalder, R. Fasel, A. Stuck, P. Aebi, L. Schlapbach, J. Electron Spectrosc. Relat. Phenom. 68 (1994) 1.
[16] R. Fasel, J. Osterwalder, Surf. Rev. and Lett. 2 (1995) 359.
[17] R.S. Williams, in: J.W. Rabalais (Ed.), Low Energy Ion–Surface Interactions, J. Wiley and Sons, Chichester, England, 1994, ch. 1, pp. 1-54.
[18] H. Bu, M. Shi, J.W. Rabalais, Nucl. Instrum. Meth. Phys. Research B 61 (1991) 337.
[19] J. Osterwalder, T. Greber, A. Stuck, L. Schlapbach, Phys. Rev. B 44 (1991) 13764.